ORIGINAL PAPER

Influence of the indirect assimilation of radar reflectivity data using the ensemble Kalman filter on the simulation of a warm-sector squall line

Xuexing Qiu[1,2,3] · Chun Liu[3] · Zhixin He[2,3] · Linlin Zheng[3]

Abstract

Radar data assimilation is an important method to improve the performance of numerical models in severe convective weather. In this study, the statistical relationships between the radar reflectivity intensity and the latent heat release intensity and humidity are calculated based on Weather Research and Forecasting (WRF) model forecast results. Then, they are used to convert the radar reflectivity observation data into the virtual observation of the temperature and humidity. Finally, these data are continuously assimilated to the initial field of the WRF model using the ensemble Kalman filter to simulate a warm-sector squall line process. The results show that the temperature and humidity in the strong radar echo area are adjusted after the radar reflectivity data are assimilated, and new convective echoes can be excited quickly in a short time. The indirect assimilation of the radar reflectivity data can effectively improve the forecast skills of both the warm-sector squall line and the influence time of the squall line. After the assimilation, the forecast results of the influence time of the squall line on the downstream regions are basically consistent with the observations. At the same time, the forecast skills of the squall line intensity and the surface gust intensity are improved. The forecast results of the experiments with different influence radii are all better than those without radar reflectivity assimilation. When the influence radius is smaller, the improvement lasts longer. When the influence radius is larger, the improvement is more significant in the now-casting period with a shorter duration. The simulation skill of this squall line is high with an influence radius of 25 km. In addition, the assimilation of the virtual observation of both the temperature and humidity can improve the forecast skill of the squall line, especially the virtual observation with the assimilation of the humidity.

1 Introduction

Doppler weather radars can monitor the occurrence and the location of thunderstorms in time. How to improve the forecast skill of the numerical model for thunderstorms and other severe convective weather by quantitatively applying radar observation data to numerical forecasts has always been a hot topic. However, there are still many problems

with the application of radar data in operational weather forecasts (Fabry and Meunier 2020). The observation operator of radar radial wind is relatively mature, and it has been widely tested and used in various assimilation methods (Xue et al. 2000; Gao et al. 2004; Xiao et al. 2005; Kuo et al. 2005; Zhao and Xue 2009; Montmerle and Faccani 2009; Wen and Zhang 2012; Chen et al. 2014; Shen and Min 2016; Shen et al. 2017a, b, 2019a, b).

The observation operator of radar reflectivity is more complicated, and there are many assimilation methods of the radar reflectivity (Zhang 1999; Snyde and Zhang 2003; Zhang et al. 2004; Sun 2005; Tong and Xue 2005; Anderson and Collins 2007; Aksoy et al. 2009, 2010; Caumont et al. 2010; Takemi 2010; Dowell et al. 2011; Sun and Wang 2013; Wang et al. 2013a, b; Wattrelot et al. 2014; Gao and Stensrud 2012, 2014; Gao et al. 2016; Wang and Wang 2017), including cloud analysis method, latent heat forcing method, variational assimilation and ensemble Kalman filter (EnKF). Radar reflectivity observation information was used

✉ Zhixin He
18156531161@163.com

1 School of Earth and Space Sciences of University of Science and Technology of China, Hefei 230026, Anhui, China

2 Shanghai Typhoon Institute of China Meteorological Administration, Shanghai 200030, China

3 Anhui Meteorological Observatory, Hefei 230031, Anhui, China

to improve the temperature, humidity fields and cloud physical parameters of the initial field, such as rain, ice water, and snow water content. Many studies have shown that the duration of the model improvement is short if the cloud physical parameters are adjusted. However, it is longer if the temperature and humidity profile or the potential temperature profile is improved (Ge et al. 2013). Improving the temperature and humidity analysis is important assimilating radar reflectivity. Xue et al. (2003), Brewster (2015), Hu et al. (2006) and Schenkman et al. (2011) have shown success in simulating and forecasting convective storms by adjusting the relative humidity, water vapor mixing ratio and temperature in the model based on radar, satellite and ground observation data during cloud analysis. Xiao et al. (2007a, 2007b) proposed a direct assimilation method of radar reflectivity data, which used the total water condensate as the humidity control variable to assimilate the radar reflectivity data directly and improved the quantitative precipitation forecast. In the short-term forecast and nowcast for the London 2012 Summer Olympics, Lee (2013) applied the latent heat data retrieved from the assimilation of the radar reflectivity data to absorb the observation information in the radar reflectivity data in the high-resolution model (1.5 km) of the Met Office. Wang et al. (2013a) assimilated retrieved rainwater and estimated in-cloud water vapor instead of assimilating radar reflectivity directly using 3DVAR method in WRF. It was concluded that on average the assimilation of reflectivity significantly improves the short-term precipitation forecast skill up to 7 h. Fan et al. (2013) used three-dimensional variational method in the Beijing rapid updated cycling analysis and forecast system to assimilate the rain and water vapor data derived from the radar reflectivity data, which greatly improved the short-term precipitation forecast skill and extended the lead time to 6 h with positive forecast skills. He et al. (2021) adjusted the humidity profile of the model initial field based on the statistical relationship between the radar reflectivity and the humidity profile and found that this method can significantly improve the short-term forecast and nowcast skills of heavy rainfall. In addition, Weygandt et al. (2008) used the diabatic digital filter initialization method in the high-resolution rapid refresh system. In the radar reflectivity factor assimilation method of the real-time four-dimensional data assimilation, the reflectivity factor was converted into the rainwater mixing ratio, and then, the latent heat was deduced based on the difference between the model simulated and observed rainwater mixing ratio. Finally, the latent heat was used as the observation data to be assimilated into the model by nudging so that the spin-up time can be reduced and the short-term forecast and nowcast skills can be improved in the model.

EnKF assimilation method has the advantage of background error covariance flow dependence. As mentioned above, assimilation radar reflectivity by EnKF can improve the short-term forecast and nowcast skill of the thunderstorm. But there are still some practical issues to consider. First, the direct radar reflectivity assimilation depends on observation operator, which is the microphysical scheme. Due to the huge amount of radar observation and the highly complex observation operator, real-time radar reflectivity assimilation would be affected by extensive computation. On the other hand, the excessive adjustment of the temperature should be avoided when the temperature and humidity profiles are adjusted for radar reflectivity indirect assimilation, it may result in integration unstable of the numerical model.

To avoid huge computation and integral instability may cause by radar reflectivity assimilation, a simple method was introduced in which the reflectivity information was converted into the temperature and humidity "virtual observation" based on the operational radar three-dimensional mosaic and the high-resolution model forecast results with the same parameterization schemes. The feasibility of the method is verified using EnKF assimilation temperature and humidity "virtual observation" for a warm zone squall line case.

The next section is the overview of the squall line case. The methods for retrieving temperature and humidity "virtual observation" are introduced in Sect. 3. Improvements of EnKF analysis field and prediction results and various sensitivity experiments results was showed in Sect. 4. Summary and conclusions follow in Sect. 5.

2 Overview of the squall line case

This squall line was occurred in the southern Anhui Province at 00:00 (UTC, the same below) to 12:00 on May 18, 2018, resulting in a large area of the thunderstorm and the wind speed exceeding 24.5 m/s. It can be seen from geopotential height at 500 hPa and wind at 850 hPa at 00:00 on May 18 (Fig. 1) that the main part of the squall line was near contour 584 gpm on the edge of the subtropical high. The low trough in Northeast China moved eastward and southward, and the low trough at 850 hPa moved eastward to the area from the Sea of Japan to the east coast of China. From 850 to 500 hPa, the southwesterly wind in front of the trough prevailed in the squall-line area. Although the low-level jet was far away from the squall-line area, the warm moist advection was still significant, and thus, the geopotential instability is strong in the squall-line area. Therefore, due to the infiltration of the cold air near the surface and the effect of the topography, the convective cells were first excited in eastern Hubei Province and the junction area of Anhui and Jiangxi Provinces. It is a typical warm-sector squall line, it is still difficult to predict it accurately.

The evolution of the squall line can be clearly seen from the radar composite reflectivity (Fig. 2). Before 02:00 on
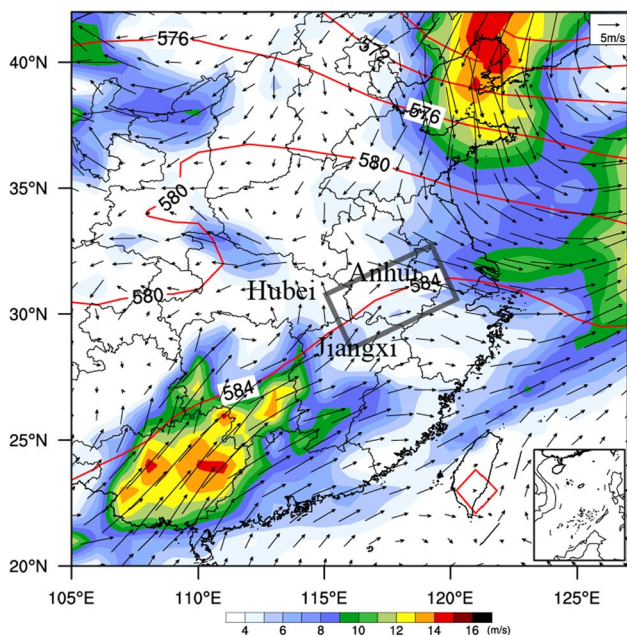
Fig. 1 The 500 hPa geopotential height (solid line) and 850 hPa wind (arrow) at 00:00 (universal time) on May 18, 2018. The shades represent the 850 hPa wind speed, and the thick black box represents the main area of the squall line

May 18, scattered convective echoes first appeared in eastern Hubei and eastern Jiangxi Provinces. At 04:00, these echoes moved to Anhui Province and began to strengthen. At the same time, some scattered convective echoes appeared in southern Anhui Province due to the strong potential instability. Then, under the influence of the southwesterly steering airflow in front of the trough, the convective echo moved from the southwest to northeast and gradually strengthened, forming an organized bow-shaped echo. At 07:00–09:00, it reached the maximum and caused a large area of thunderstorms and gusts on the surface. After 10:00, the squall line gradually weakened during the eastward movement due to the energy consumption. When it moved to Jiangsu Province at 12:00, the composite reflectivity decreased to below 40 dBZ, and the squall line weakened and dissipated. In this process, the squall line was generated and dissipated in the warm sector in front of the trough and moved northeastward under the influence of the southwesterly steering airflow. Next, we will take the squall line process as the research object to analyze the impact of EnKF assimilation temperature and humidity "virtual observation" converted from radar reflectivity on the squall line nowcasting.
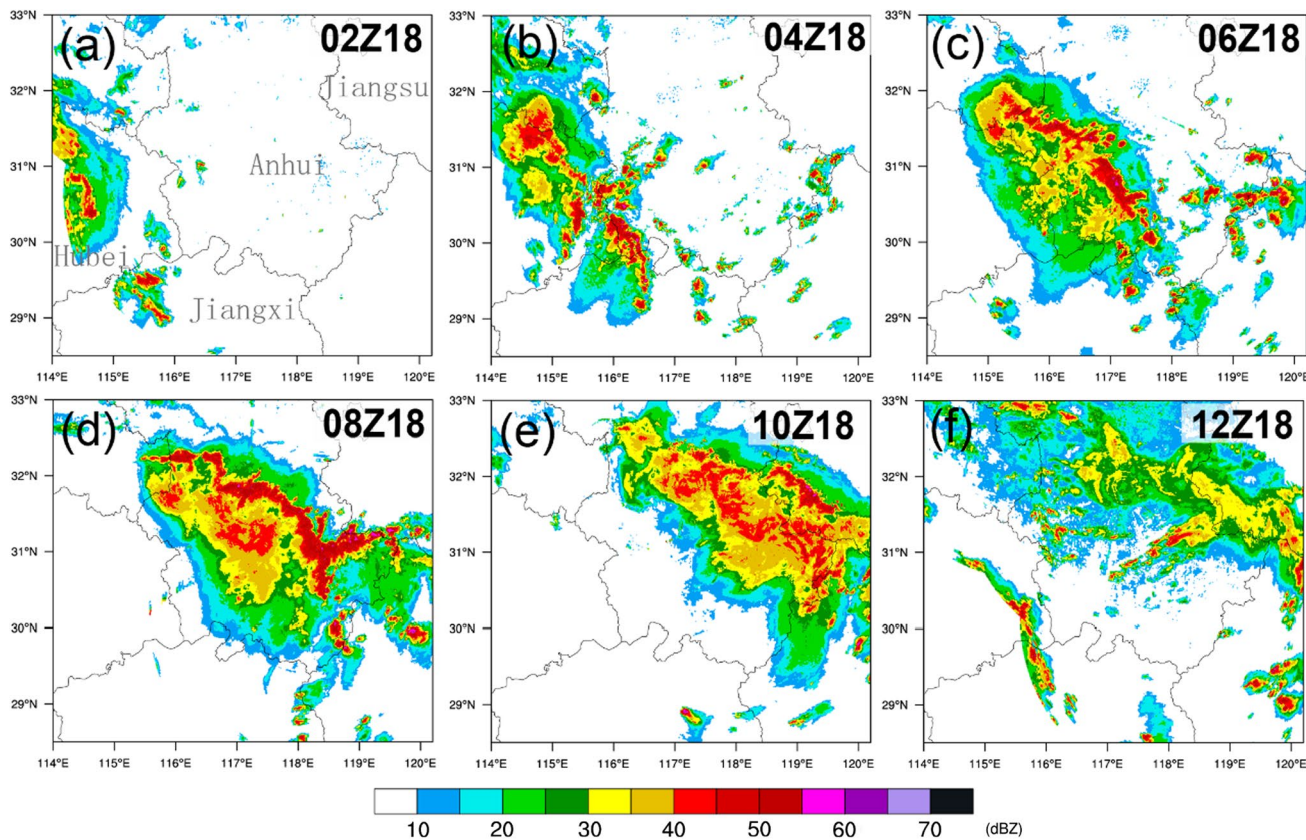
Fig. 2 Composite reflectivity at **a** 0200, **b** 0400, **c** 0600, **d** 0800, **e** 1000 and **f** 1200 UTC 18 May 2018

Table 1 Regression coefficients of different levels

| Level (hPa)	a0	a1	a2	a3
400	0.515	− 0.087	0.021	− 0.003
500	− 0.996	− 0.178	0.027	0.007
550	− 0.287	− 0.158	0.022	0.012
600	0.188	− 0.190	0.003	0.014
650	1.283	− 0.140	0.0	0.017
700	1.260	− 0.093	− 0.006	0.018
750	0.869	− 0.096	− 0.002	0.109
800	1.371	− 0.242	− 0.009	0.011
850	4.742	− 0.142	− 0.013	0.005
900	1.561	− 0.04	− 0.013	0.020
925	− 0.106	− 0.04	− 0.017	0.014
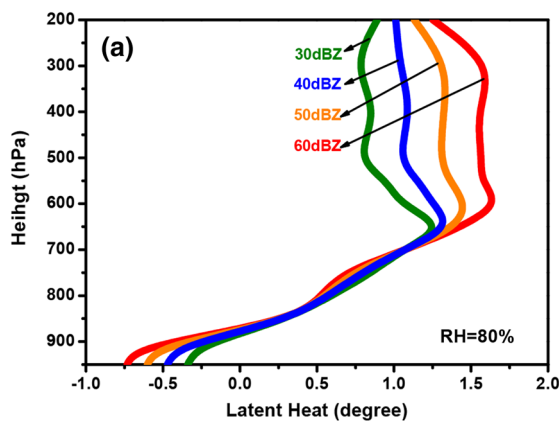
environment temperature(ΔT), and the reflectivity intensity, environment temperature and environment humidity during the convective development. The calculation formula is

$$\Delta T = F(\text{RF}, T, \text{RH}) = a_0 + a_1 \times \text{RF} + a_2 \times T + a_3 \times \text{RH}$$

where RF was simulated radar reflectivity(dBZ) by WRF, and T was environment temperature (K) and RH was relative humidity (%). T and RH were the average temperature and relative humidity within a radius of 15 km respectively. Different pressure levels (400 hPa, 500 hPa, 550 hPa, 600 hPa, 650 hPa, 700 hPa, 750 hPa, 800 hPa, 850 hPa, 900 hPa, 925 hPa) are calculated separately.

The regression coefficients of different levels are shown in Table 1.

To statistically analyze of atmospheric saturation in the
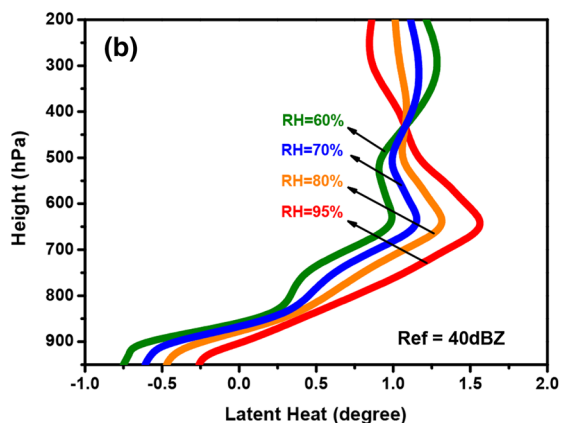
Fig. 3 The statistical relationship of the latent heat release intensity against the background of the typical summer temperature profile. **a** The variation of the latent heat release intensity with the variation in the reflectivity intensity at different heights when the relative humidity is 80%. **b** The statistical relationship between the latent heat release intensity and the relative humidity at different heights when the reflectivity is 40 dBZ

3 Methods, data, and experiment design

3.1 The method of retrieving the latent heat using the radar reflectivity

Before the indirect assimilation of radar reflectivity data using the EnKF, it is necessary to establish statistical relationships between the radar reflectivity intensity and the latent heat release and humidity under different environment conditions. As it is difficult to accurately simulate the intensity and location of the radar reflectivity using the numerical model, this study uses the radar reflectivity diagnosed based on cloud physical parameters simulated using the Weather Research and Forecasting (WRF) model as statistical samples to calculate the quantitative statistical relationships between the latent heat release intensity, expressed by the difference between the single-point temperature and the

strong echo area, we statistically analyze the relative humidity at different heights of the model according to 5 dBZ intervals. It is found that between the lifting condensation level and the 0 ℃ altitude, when the radar reflectivity simulated by the model exceeds 25 dBZ, the relative humidity of the atmosphere exceeds 95%.

The real-time 12–36 h forecast results every 12:00 during May–August of 2017–2019 are used as the statistical samples. Against the background of the typical summer temperature profile, the variation of the potential release intensity with the variation in the reflectivity intensity and relative humidity at different pressure heights is shown in Fig. 3. The latent heat release is positive above 850 hPa. The maximum intensity of the potential release occurs between 600 and 300 hPa with a maximum of approximately 1.5 ℃, and it increases with the reflectivity intensity. The potential release intensity between 850 and 600 hPa is insensitive to
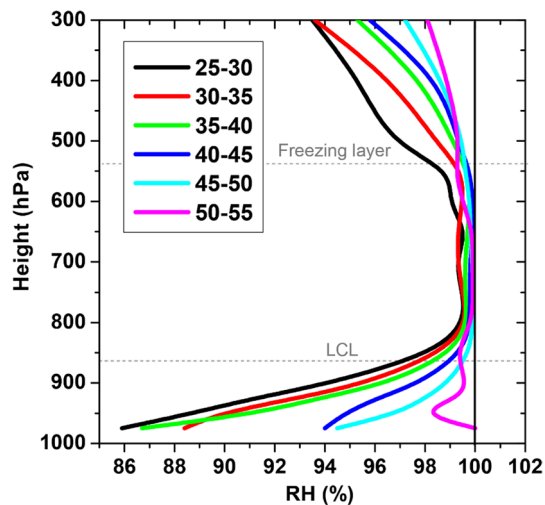
Fig. 4 The statistical relationship between the relative humidity and the reflectivity intensity at different heights

Fig. 5 The simulation domains (D1, D2) of WRF, shading represents topography (units: meters)

the reflectivity intensity, but it increases with the height. The potential release is mainly negative below 850 hPa, which may be caused by the mid-upper-level sinking of the low-level radar echo in the model. In the sinking process, the evaporation and heat absorption caused by the incoming dry air makes the storm temperature lower than the environment temperature, and the storm is in the declining stage. In addition, Fig. 3b shows that the latent heat release intensity increases with the relative humidity below 400 hPa. Above 400 hPa, the situation is the opposite.

The statistical relationship between the relative humidity and the reflectivity intensity at different heights is shown in Fig. 4. It shows that when the reflectivity intensity exceeds 25 dBZ between the lifting condensation level and the freezing level, the relative humidity is within 98–100%. In other words, the atmosphere is close to saturation when the intensity is more than 25 dBZ in this height range. However, below the lifting condensation level and above the freezing level, the atmosphere is closer to saturation with the increase in reflectivity, but the large span of the relative humidity indicates great uncertainty in the atmospheric saturation.

Based on the above statistical results and the radar reflectivity observation data after the quality control and sparseness process, the temperature and humidity of the model forecast are used as the environment temperature and humidity to calculate the latent heat release intensity in the radar reflectivity assimilation using the EnKF, and thus, the virtual observation of the temperature at the height of the radar echo is obtained. Then, it is analyzed whether the echo height is between the lifting condensation level and the freezing level. If the echo is between the two levels, the atmosphere is considered to be saturated, and a virtual observation of the dew point temperature is achieved. Finally, in the area without
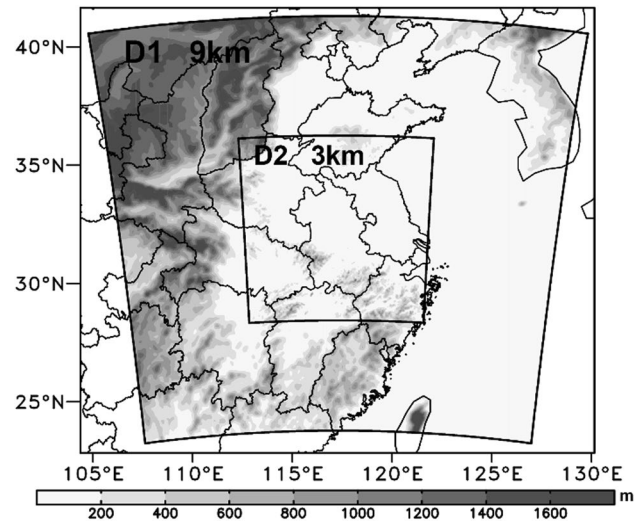
a convective echo in the forecast but with a strong echo in the observation, the virtual observation of the temperature and humidity is assimilated to the initial field of the WRF model using the EnKF. Specifically, the observation error of the temperature and dew point temperature is defined as 1℃ in this study.

3.2 Assimilation system and forecast model

The EnKF used in this paper is developed by Pennsylvania State University (Zhang et al. 2006a, 2009, b; Meng and Zhang 2007, 2008a, b), and contains 32 ensemble members. The initial disturbance is generated in domain 01 using the background error covariance option cv3 in the WRF data assimilation system (Barker et al. 2004), then, the initial disturbance is downscaled to domain 02 using the WRF model. The background error covariance expansion method developed by Zhang et al. (2004) is used, and the weight coefficient is 0.75. The model forecast error is represented by the stochastic combination of multi-physical process parameterization schemes (Meng and Zhang 2007; Lan et al. 2010b).

The forecast model is WRF V3.8 (Skamarock et al. 2005). A double nesting scheme is used to represent the model area with resolutions of 9 km and 3 km, and the grid numbers are 229×217 and 289×289, respectively (Fig. 5). There are 35 levels in the vertical direction of the model with a top-level of 50 hPa. The same parameterization schemes are used in the deterministic forecast, and the WSM6 parameterization scheme is used in the microphysical process (Hong et al. 2004). The YSU parameterization scheme is used in the boundary layer process (Noh et al. 2003), and the Kain–Fritsh parameterization scheme is used in the cumulus parameterization scheme. The real-time analysis and forecast
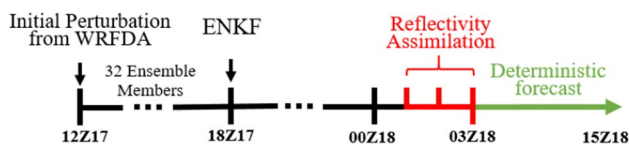
Fig. 6 Schematic chart of the WRF-EnKF numerical experiment

Table 2 Settings of the sensitivity numerical experiments

No	Experiment	Description
1	CNTL	Controlled experiment, which assimilates the conventional observation and radar radial wind observation data without assimilating the radar reflectivity data
2	REF05	Assimilate the radar reflectivity data with the influence radius of 5 km
3	REF15	Assimilate the radar reflectivity data with the influence radius of 15 km
4	REF25	Assimilate the radar reflectivity data with the influence radius of 25 km
5	REF35	Assimilate the radar reflectivity data with the influence radius of 35 km
6	REF_T	Same as REF25, but only considers the effect of the reflectivity on the temperature
7	REF_Q	Same as REF25, but only considers the effect of the reflectivity on the humidity

data provided by the European Centre for Medium-Range Weather Forecasts to the China Meteorological Administration are used as the initial field and boundary conditions of the model, including the surface layer and 19 pressure levels, that is, 1000 hPa, 950 hPa, 925 hPa, 700 hPa, 600 hPa, 500 hPa, 400 hPa, 300 hPa, 250 hPa, 200 hPa, 150 hPa, 100 hPa, 70 hPa, 50 hPa, 20 hPa, and 10 hPa. The horizontal resolution of the surface level is 0.125°, and that of the pressure level is 0.25°. The lateral boundary conditions are updated every 3 h. The disturbance mode of the lateral boundary is the same as that of the initial condition.

3.3 Design of the numerical experiment

To simulate this warm-sector squall line process, the schematic chart of the experiment is shown in Fig. 6. This process mainly occurred in the afternoon on May 18, thus, the WRF-EnKF system starts at12:00 on May 17. First, the initial disturbance is generated using the cv3 option of the WRF data assimilation system, and the observation data are assimilated at 18:00 after 6 h of integration. Since convective echoes appear in the simulation area at 01:00 on May 18, the radar reflectivity data are indirectly assimilated three times continuously from 01:00 to 03:00 on May 18. Then the ensemble mean field assimilated using the EnKF at 03:00 is taken as the initial field for the deterministic forecast.

To analyze the influence of the EnKF indirect assimilation of the radar reflectivity data on the squall line process, 7 sets of numerical experiments are designed (Table 2). As the observation operators of conventional surface observation, sounding observation and radar radial wind observation are relatively mature, assimilation using the WRF-EnKF system is well-developed for these data, and the experiment is used

as the controlled experiment (CNTL). Based on the CNTL, the radar reflectivity data are indirectly assimilated as the reference experiment (REF) to analyze the effect of the assimilation of the reflectivity data. To evaluate the impact of different influence radii on the forecast skill, four sets of experiments are designed with different influence radii. In addition, to study whether improving the temperature pro-

file or the humidity profile in the radar reflectivity assimilation has a more significant influence on the forecast results, REF_T and REF_Q are designed. The former only considers the influence of the radar reflectivity on the temperature profile, while the latter only considers the influence of the radar reflectivity on the humidity profile.

4 Results

4.1 Comparison of the analysis fields

The experiment results with different influence radii show that the simulation skill of the experiment with an influence radii of 25 km is high, namely REF25. Therefore, REF25 and CNTL are compared and analyzed to discuss the EnKF indirect assimilation of the radar reflectivity data. Figure 7 shows the comparison of the radar observation with the composite reflectivity analysis results of REF25 and CNTL. By 01:00 on May 18, scattered convective echoes were generated in the simulated area. However, in the convective echo simulated by the WRF model, because the control variables in the EnKF assimilation do not contain various cloud physical parameters, the analysis field will not change the composite reflectivity based on the cloud physical parameters. Therefore, the composite reflectivity results of the two analysis fields are exactly the same (Fig. 7b1 and c1). After 1:00, the radar reflectivity data are assimilated, and then, the forecast continues for another hour. The results show that there are new convective echoes in the region, but the forecasted location is inaccurate. By 03:00 on May 18, the convective echo moved to the border of Anhui, Hubei,
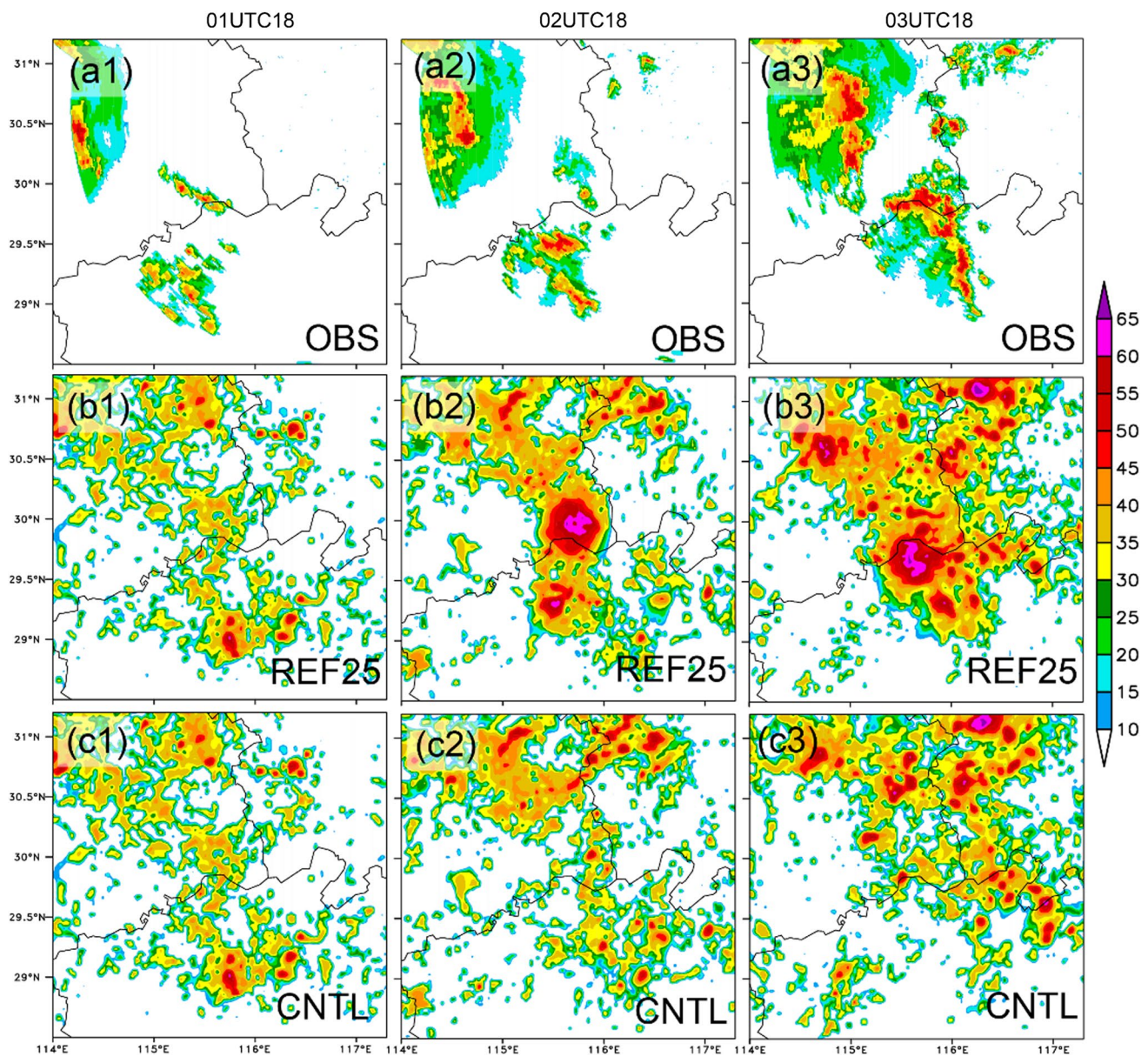
Fig. 7 Observed composite reflectivity (a1-3) and composite reflectivity analysis of REF25 (b1-3) and CNTL (c1-3) at 01,02 and 03UTC 18 May 2018

and Jiangxi Provinces. In the CNTL, the convective echoes have moved to Anhui Province, which is to the east of the observation, with a lower intensity. After radar reflectivity data assimilation using the EnKF two consecutive times, the convective echo location is more accurate, but the intensity is higher than that of the observation.

The difference in the temperature and relative humidity analysis fields between CNTL and REF25 in Fig. 8. The horizontal difference at 500 hPa (Fig. 8a) shows that the temperature and humidity of REF25 in the convective area are higher than those of CNTL due to radar reflectivity data assimilation. Specifically, the maximum increase of

the temperature is close to 1℃, and the maximum increase in relative humidity is approximately 40%. The areas with the increasing temperature and the increasing relative humidity are both in the strong echo area, indicating the effect of the radar reflectivity assimilation. The vertical distribution (Fig. 8b) shows that the relative humidity increases significantly within 850–400 hPa, with the maximum difference near 500 hPa, while the maximum temperature difference appears within 800–700 hPa. The inconsistency of the large difference centers of the temperature and relative humidity may be induced by the relative humidity at the mid-lower level of the first guess field,
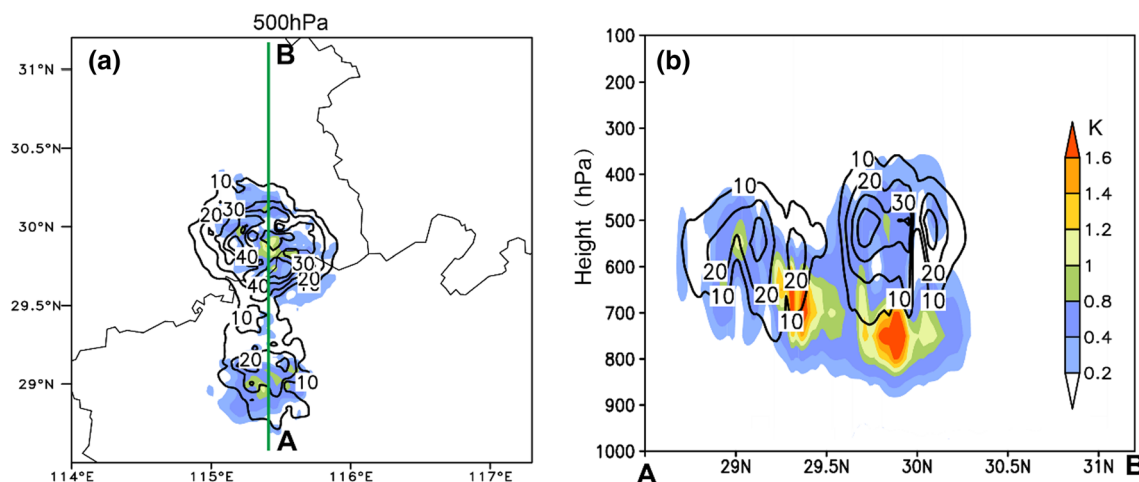
Fig. 8 The difference of the temperature and humidity analysis fields between the CNTL and the REF25 on 03UTC 18 May 2018. **a** 500 hPa, **b** the plane along AB in (**a**), the shades represent the temperature and the contours represent the relative humidity

which is close to saturation and it is impossible to adjust the relative humidity. However, despite the strong echo at low levels, the low relative humidity in the middle level of the first guess field can affect the middle level through the vertical covariance.

In summary, using the EnKF to assimilate the virtual observation information of the temperature and humidity retrieved from the radar reflectivity and adjusting the temperature and humidity profiles in the convective area, new convective echoes can be quickly excited in the convective region to provide more accurate small and medium scale information for subsequent forecasts.

4.2 Comparison of the forecast fields

The above analyses show that the EnKF can indirectly assimilate the radar reflectivity data to excite new convective echoes in the convective area. Are these new convective echoes closer to the observation? At 03:00 on May 18, the EnKF ensemble mean fields of CNTL and REF25 are used as the initial field of the WRF model for the 12 h forecast, and the composite reflectivity forecast fields of the 1st, 3rd, and 5th hours are shown in Fig. 9.

Compared with CNTL, the location of the squall line forecasted by REF25 is more accurate with higher intensity after the radar reflectivity data assimilation in Fig. 9. For example, at 06:00 on May 18, the squall line was between the Anqing radar and the Tongling radar, while the convective echo forecasted by CNTL moved over the Tongling radar. In comparison, the location of the radar echo forecasted by REF25 is more accurate. Meanwhile, at 08:00 on May 18, the squall line forecasted by CNTL has moved past the Hefei radar, but in the observation, it just moves close to

the Hefei radar. The convection occurrence time by REF25 is more consistent with the observation, and the intensity is also higher.

To quantitatively evaluate the influence of the radar reflectivity data assimilation on the forecast, the equitable threat score (ETS) of the composite reflectivity of the two experiment forecasts are calculated initiated at 01:00, 02:00, and 03:00 on May 18 (Fig. 10), which are recorded as ETS01, ETS02 and ETS03, respectively. For radar echoes over 30 dBZ (Fig. 10a), ETS01 is significantly improved after assimilating the composite reflectivity data once, and the improvement can last for more than 9 h to 10:00 on May 18. Compared with ETS01, ETS02 is higher in the first 6 h to 08:00 on May 18 after the second assimilation of the composite reflectivity data. ETS03 is still slightly higher than ETS01 and ETS02 in the first 4 h to 07:00 on May 18 after the third assimilation of the composite reflectivity data. For 40 dBZ (Fig. 10b), the ETS values after the composite reflectivity data assimilation are generally higher than those of CNTL results without assimilation until the squall line began to weaken at 10:00 on May 18.

And we also found that the ETS03 is not always the highest at all lead times, for example, ETS03 at 30 dBZ is lower than ETS01 and ETS02 after a 4 h lead time. Similar results are found in CNTL. The similar result appeared in other studies of water vapor assimilation (Schenkman et al. 2011a, b), and the large and strong convective range of the analysis field may be the main reason.

The thunderstorm and gust induced by the squall line are the main causes of the disasters, thus, the accurate forecast of the gust intensity is particularly important for the early warning. The comparison of the maximum wind speed of each integration step forecasted by the WRF model (Fig. 11) shows that although the CNTL can better
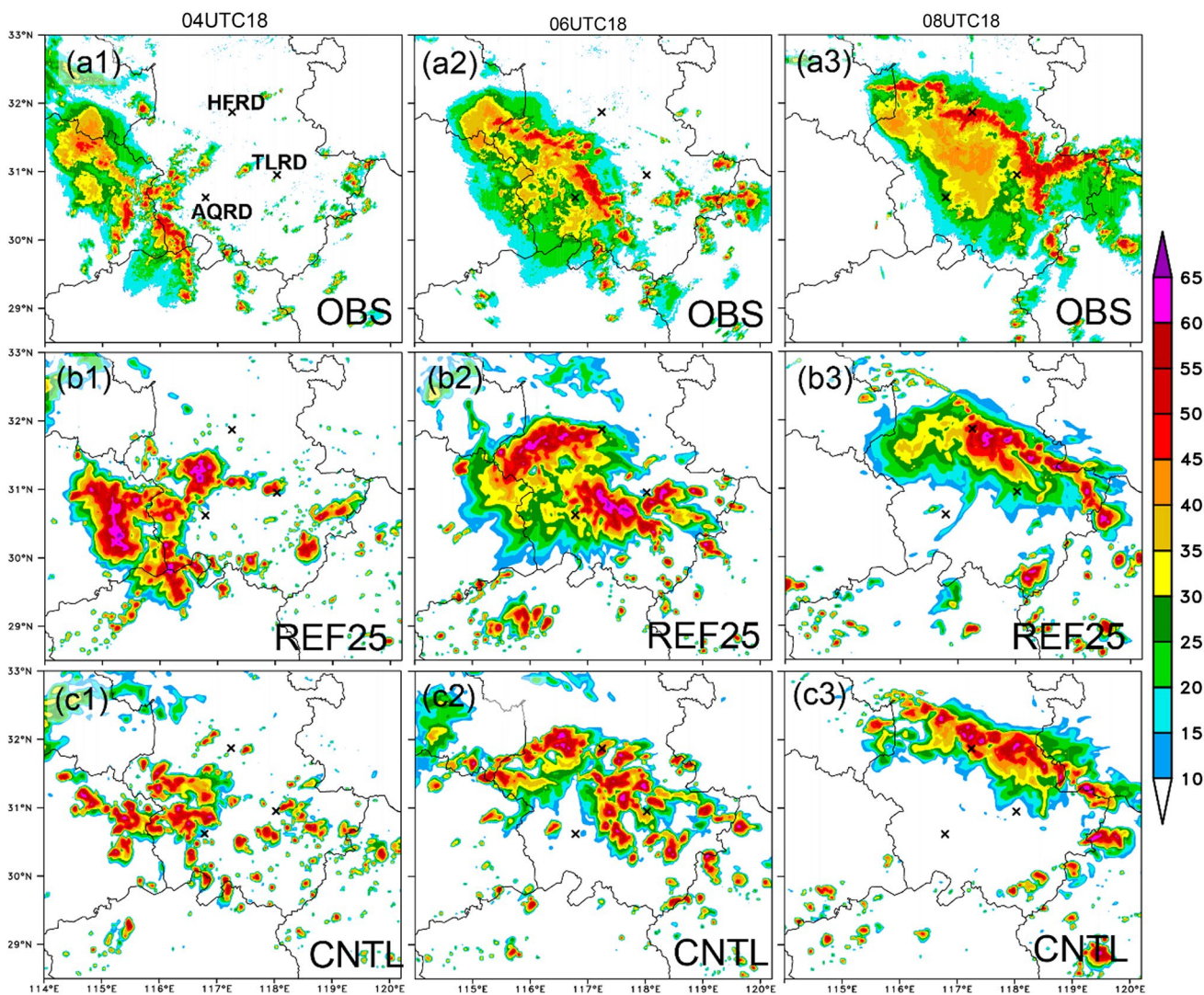
Fig. 9 Observed composite reflectivity (a1-3) and simulated composite reflectivity of REF25 (b1-3) and CNTL (c1-3) initial at 03UTC 18 May 2018. AQRD, TLRD, and HFRD marked with × represent the locations of the Anqing radar, Tongling radar, and Hefei radar location, respectively

forecast the eastward movement of the squall line gust, the forecasted intensity is lower and the range is smaller than the observation. A large area of the thunderstorm gust over 18 m s^{-1} occurs in the observation, while the CNTL only forecasted a small area of the gust over 14 m s^{-1}. Moreover, the forecasted location of the radar echo is to the east of the observation, and the forecasted gust appears earlier than the observation. After the radar reflectivity data assimilation, the forecasted intensity, location, and area of the gust are significantly more accurate than those of the CNTL, although the gust area is still smaller than the observation. The gust is observed in areas with the forecasted gusts over 18 m s^{-1}.

Therefore, the indirect assimilation of the radar reflectivity using the EnKF can significantly improve the forecast results. The forecasted intensity of the squall line is improved, and the forecasted intensity and range of the hourly maximum wind speed on the surface are closer to the observation than before. The assimilation also improves the accuracy of both the forecasted location of the squall line and the forecasted squall line influence time. The comparison shows that the improvement induced by the assimilation in the initial stage is more significant.

4.3 Sensitivity experiment with different influence radii

The influence radius of the observation data is a very important parameter in EnKF assimilation. Which influence radius can be set to achieve the best forecast results for the virtual observation retrieved from the radar reflectivity? Four

Fig. 10 The ETS score for the simulated composite reflectivity greater than **a** 30 dBZ and **b** 40 dBZ by the CNTL and the REF25 initiated at different times
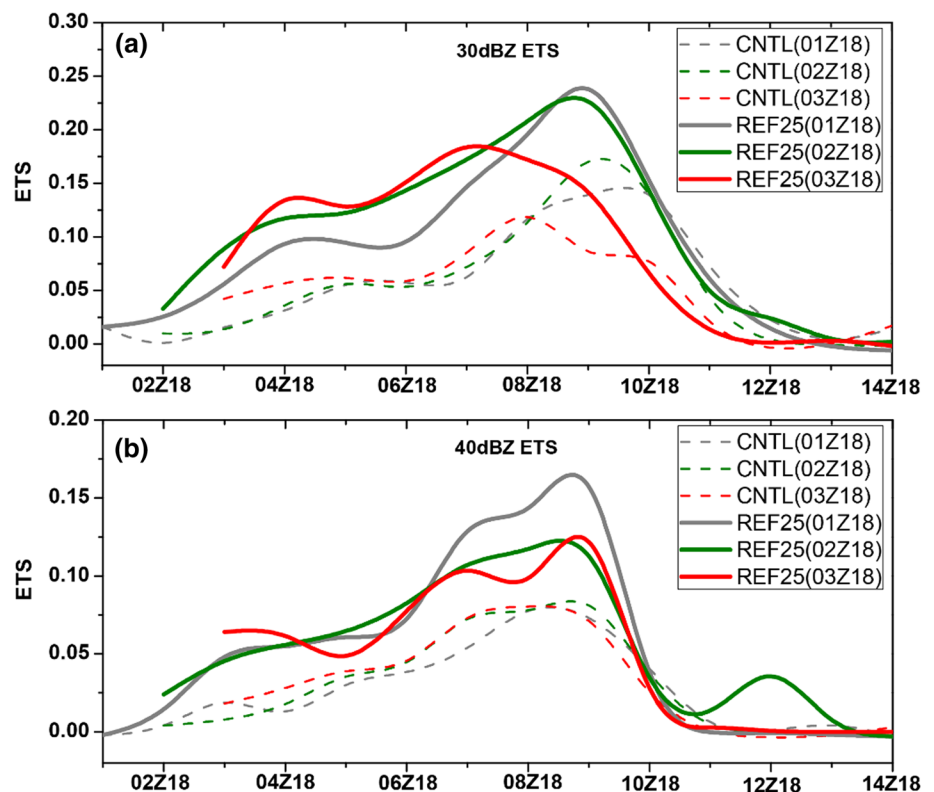

experiments with influence radius of 5 km, 15 km, 25 km, and 35 km are designed. The ETS score of four experiments initiated at 03:00 on May 18 (Fig. 12) shows that ETS values of four experiments after the radar reflectivity data assimilation are higher than those of CNTL. However, the range and duration of the ETS improvement vary with the influence radii. For experiments of this squall line case, a larger influence radii corresponds to a higher ETS and a shorter duration. A smaller influence radii corresponds to a longer duration of the improvement, but ETS is not the highest in a short period of time. For example, for radar reflectivity greater than 30 dBZ (Fig. 12a), ETS is higher than that of CNTL before 12:00 on May 18 when the influence radius is 15 km (REF15). When the influence radius is 35 km (REF35), the ETS of the first 4 h is significantly higher than those of the other three sets, but it also decreases faster after 4 h. The trend is similar for echoes above 40 dBZ (Fig. 12b). When the influence radius is too large, the intensity and coverage of convection will be over-predicted compared with the actual observation, and too much water vapor will be consumed in the environmental field, resulting in the decline of subsequent prediction performance. This result is consistent with that in relevant studies (Fierro et al. 2016), if the convection in the analysis field is too strong, it is easy to lead to a rapid decline in prediction performance.

For the hourly maximum wind speed forecast, the ETS values of exceeding 10 m s^{-1} are shown in Table 3. The ETS

values of the CNTL within 6 h are generally lower than those of the four sets of experiments. Among the four experiments, the ETS values of the REF25 and the REF35 are higher than the others. With a larger influence radius, the forecasted squall line intensity is higher, thus, the forecast skill of the surface gust is higher. With a small influence radius, such as 5 km, the small range of newly generated convective cells leads to a lower ETS score, but it does not consume too much water vapor in the environmental field, and its positive performance can be maintained for a longer time.

4.4 Sensitivity experiments of the humidity assimilation and temperature assimilation separately

Figure 13 shows the ETS score for simulated composite reflectivity greater than 30 dBZ and 40 dBZ of REF_T and REF_Q. REF_T is almost the same as that of CNTL, while the ETS of the REF_Q is basically equivalent to that of the REF25 for simulated 30 dBZ reflectivity (Fig. 13a). This indicates that adjusting the humidity profile of the initial field is more important than adjusting the temperature profile for the forecast of the composite reflectivity. For simulated 40 dBZ reflectivity (Fig. 13b), the prediction score of REF_T was lower than that of CNTL except for the first 2 h, and the ETS score of REF_Q was higher than that of CNTL for 6 h forecasts. The reason may be that when the
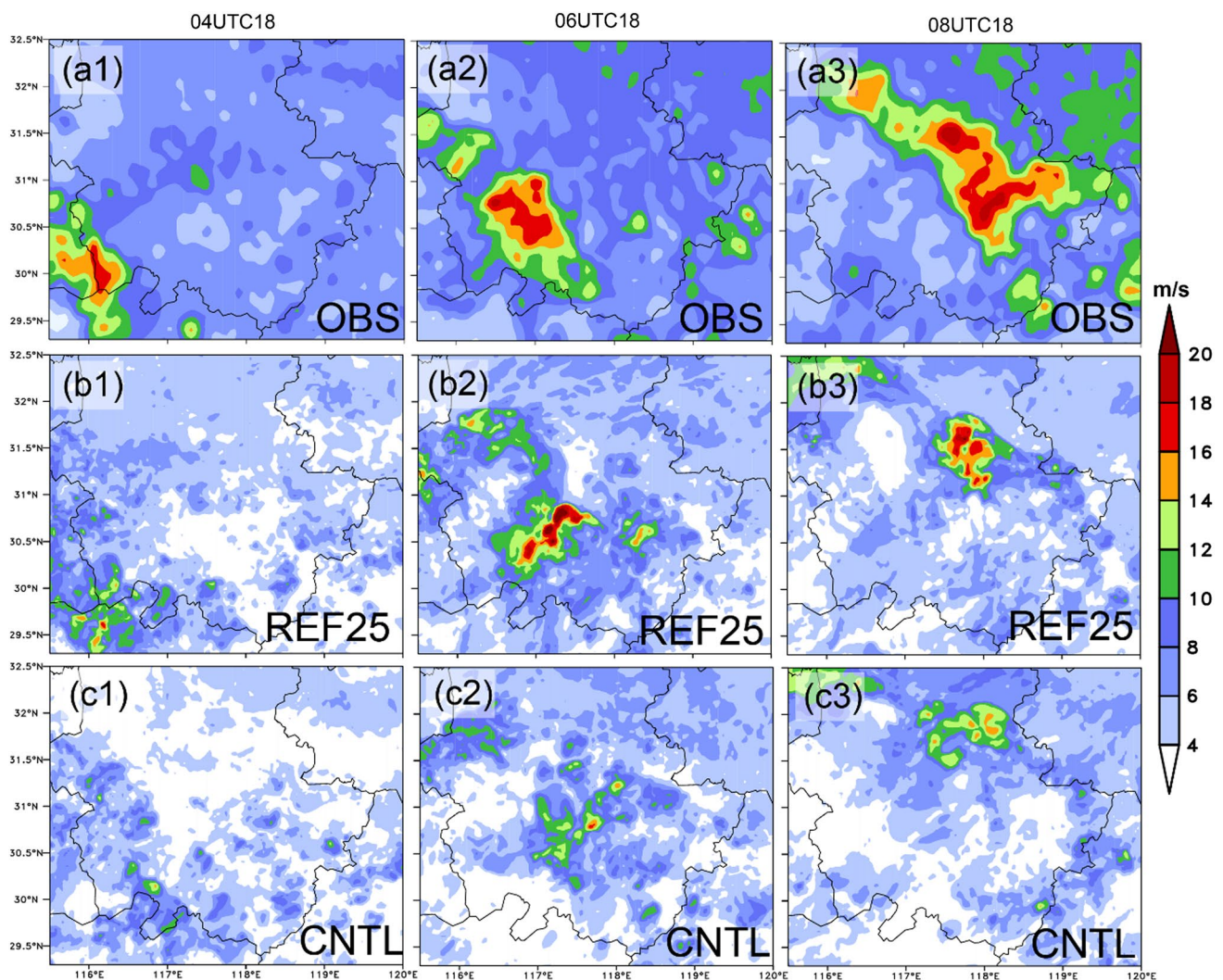
Fig. 11 Hourly maximum wind speed observation (a1-3) and simulated maximum wind speed of REF25 (b1-3) and CNTL (c1-3) initial at 03UTC 18 May 2018

temperature of the middle layer increases, the temperature lapse rate of the lower layer decreases, which is not conducive to the enhancement of convection and inhibits the development of cloud and precipitation (Takemi 2010). In addition, the latent heat statistical method adopted also has statistical errors, which may be another reason for the decline in prediction performance.

For the forecast of the hourly maximum wind speed (Table 4), the ETS values of REF_T and REF_Q are higher than that of CNTL but lower than that of REF25. This indicates that assimilating the virtual observation of the temperature or humidity retrieved from the radar reflectivity using the EnKF can improve the forecast skill of the hourly maximum wind speed. When both of them are used, the ETS is the highest and the improvement is the most significant. In contrast, the ETS of the forecast after assimilating the humidity virtual observation is closer to

that of REF25, which indicates that the adjustment of the humidity field has a more significant effect on the forecast of the squall line.

5 Summary and conclusion

An indirect assimilation technique of radar reflectivity data is described in this paper. This technique, which used latent heating specified and water vapor saturation from statistical relationship of the WRF model forecast, was evaluated through a warm-sector squall line using EnKF. This study provides documentation of the performance of the indirect assimilation technique by comparing forecast accuracy of models simulated composite reflectivity and maximum wind speed before and after assimilated radar reflectivity. New convective echoes can be quickly

Fig. 12 The ETS score for the simulated composite reflectivity greater than **a** 30 dBZ and **b** 40 dBZ of different influence radius experiments initiated at 03UTC 18 May 2018
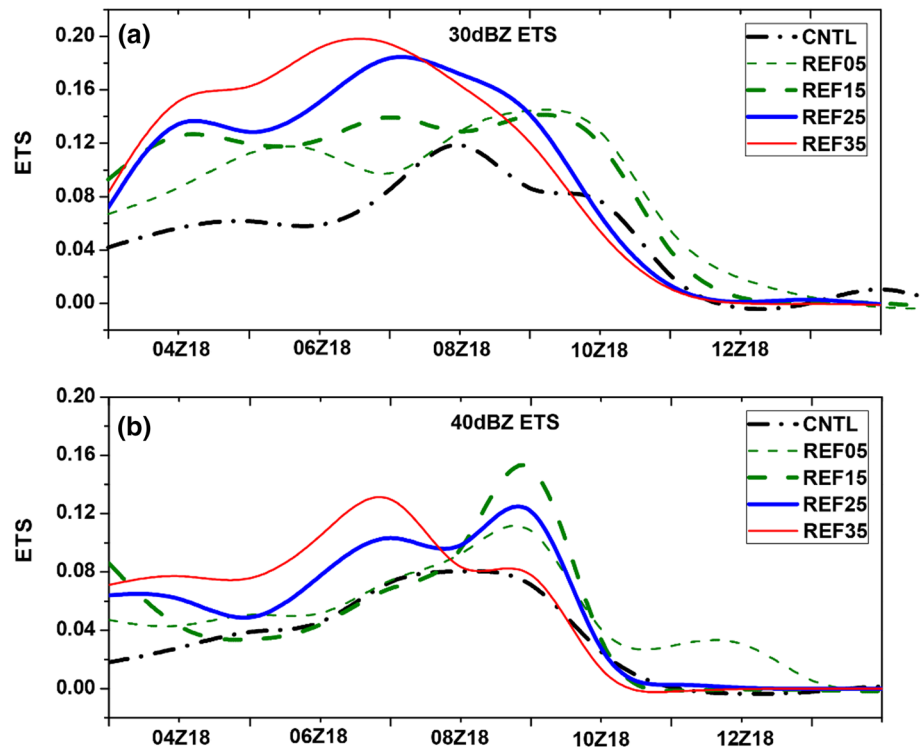
Table 3 ETS score of hourly maximum wind speed exceeding 10 m/s of different influence radii experiments initiated at 03UTC 18 May 2018

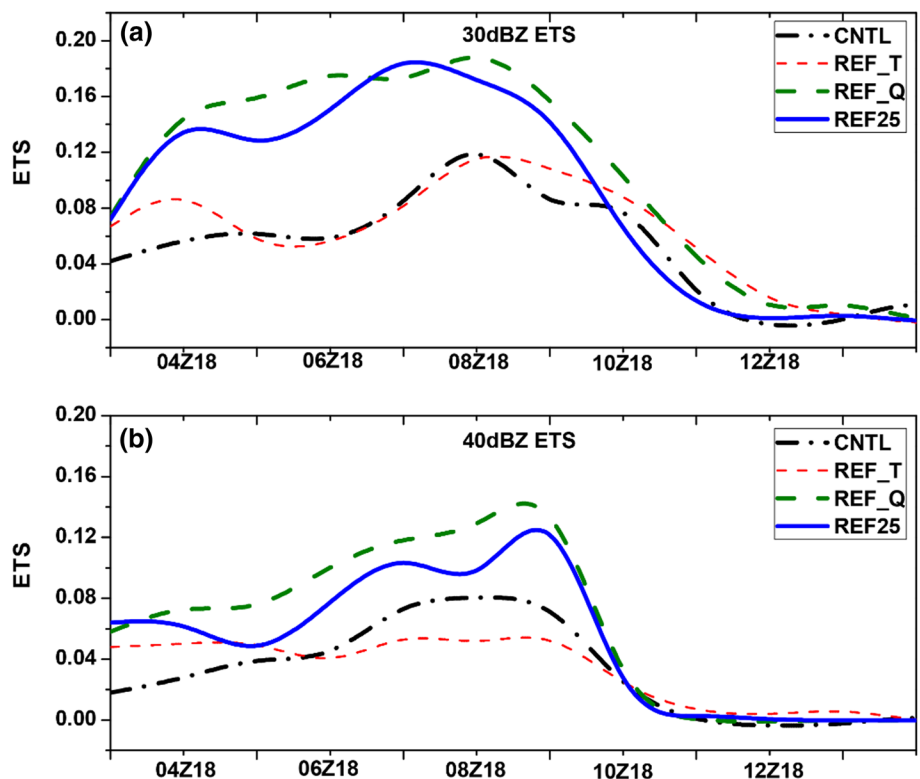|	1 h	2 h	3 h	4 h	5 h	6 h
CNTL	0.0	0.02	0.04	0.0	0.01	0.0
REF5	0.02	0.03	0.02	0.02	0.09	0.03
REF15	0.07	0.10	0.04	0.05	0.0	0.0
REF25	0.1	0.17	0.17	0.10	0.09	0.05
REF35	0.14	0.16	0.22	0.09	0.09	0.0

growing in a short time after radar reflectivity data assimilation and improved the forecast skill of the warm-sector squall line. The forecasted influence time of the squall line is more accurate so that the forecasted influence time of the squall line on the downstream regions after the radar reflectivity data assimilation is basically consistent with the observation. Moreover, the simulation of the squall line intensity is improved after the reflectivity data assimilation. The squall line intensity increases, and the intensity of the surface gust caused by the simulated squall line is closer to the observation.

Sensitivity experiments with different influence radii show that the forecasts of all experiments are better than that of CNTL without radar reflectivity assimilation. When the influence radius is small, the improvement lasts longer, while when the influence radius is large, the improvement is more significant in the nowcast period, but it lasts a shorter period. The simulation of the squall line is better than the others based on the influence radius of 25 km.

The separate assimilation experiments of the virtual observation of the temperature or humidity show that both can improve the simulation of the squall line, and the improvement of the virtual observation of the assimilated humidity is more significant. The virtual observation of the assimilated temperature can slightly improve the reflectivity simulation, while it can better improve the simulation skill of the surface gust.

Compared with the direct assimilation method of radar reflectivity, the indirect assimilation method presented in this paper avoids the complex reflectivity observation operator and reduces the indirect error caused by the uncertainty of the observation operator. Compared to other indirect assimilation methods, e.g., the latent heating method, the method has a similar forecasting effect and easier to implement. In addition, we can found that the method also has certain shortcomings, such as the lack of assimilation ability of the reflectivity information above the level of 0 ℃ and there are still original false echoes with location deviations.

Fig. 13 The ETS score for the simulated composite reflectivity greater than **a** 30 dBZ and **b** 40 dBZ of the REF_T and REF_Q initiated at 03UTC 18 May 2018

Table 4 The ETS score of hourly maximum wind speed exceeding 10 m/s of of the REF_T and REF_Q initiated at 03UTC 18 May 2018

	1 h	2 h	3 h	4 h	5 h	6 h
CNTL	0.0	0.02	0.04	0.0	0.01	0.0
REF25	0.1	0.17	0.17	0.10	0.09	0.05
REF_T	0.0	0.03	0.02	0.02	0.05	0.02
REF_Q	0.05	0.08	0.12	0.09	0.09	0.03

Future work will explore assimilating radar clear-sky echoes to eliminate false echoes. Furthermore, it is worth exploring how to make full use of the forecast information of different ensemble members to eliminate false echoes. In addition, structure of the vertical covariance in EnKF will examined in future and other weather processes, such as rainstorms and typhoons, will to be analyzed and evaluated.

References

Aksoy A, Dowell DC, Snyder C (2009) A multi-case comparative assessment of the ensemble Kalman filter for assimilation of radar observations. Part I: storm-scale analyses. Mon Weather Rev 137:1805–1824

Aksoy A, Dowell DC, Snyder C (2010) A multi-case comparative assessment of the ensemble Kalman filter for assimilation of radar observations. Part II: short-range ensemble forecasts. Mon Weather Rev 138:1273–1292

Anderson JL, Collins NS (2007) Scalable implementations of ensemble filter algorithm s for data assimilation. J Atmos Oceanic Technol 24:1452–1463

Barker DM, Huang W, Guo YR et al (2004) A three-dimensional variational data assimilation system for MM5: implementation and initial results. Mon Weather Rev 132:897–914

Brewster KA (2015) An updated high resolution hydrometeor analysis system using radar and other data 27th Conf on Weather Analysis and Forecasting 23rd Conf on numerical weather prediction Chicago IL. Amer Met Soc 31:19

Caumont O, Ducrocq V, Wattrelot E et al (2010) 1D13DVar assimilation of radar reflectivity data: a proof of concept. Dynamic Meteorol Oceanogr 62:173–187

Chen M, Chen M, Fan S (2014) The real-time radar radial velocity 3DVar assimilation experiments for application to an operational forecast model in North China. Acta Meteorol Sin 72(4):658–677

Dowell DC, Wicker LJ, Snyder C (2011) Ensemble Kalman filter assimilation of radar observations of the 8 May 2003 Oklahoma City supercell: Influences of reflectivity observations on storm-scale analyses. Mon Weather Rev 139:272–294

Fabry F, Meunier V (2020) Why are radar data so difficult to assimilate skillfully? Mon Weather Rev 148:2819–2835

Fan S, Wang H, Chen M, Gao H (2013) Study of the data assimilation of radar reflectivity with the WRF 3D-Var[J]. Acta Meteorol Sin 71(3):527–537

Fierro AO, Gao JD, Ziegler CL et al (2016) Assimilation of flash extent data in the variational frame work at convection-allowing scales: proof of concept and evaluation for the short term forecast of the 24 May 2011 tornado outbreak[J]. Mon Weather Rev 144(11):4373–4393

Gao JD, Stensrud DJ (2012) Assimilation of reflectivity data in a convective-scale, cycled 3DVAR framework with hydrometeor classification. J Atmos Sci 69:1054–1065

Gao JD, Stensrud DJ (2014) Some observing system simulation experiments with a hybrid 3DEnVAR system for storm-scale radar data assimilation. Mon Weather Rev 142:3326–3346

Gao JD, Xue M, Brewster K et al (2004) A three-dimensional variational data analysis method with recursive filter for Doppler radars. J Atmos Ocean Technol 21:457–469

Gao JD, Fu CH, Stensrud DJ et al (2016) OSSEs for an ensemble 3DVAR data assimilation system with radar observations of convective storms. J Atmos Sci 73:2403–2426

Ge G, Gao JD, Xue M (2013) Impacts of assimilating measurements of different state variables with a simulated supercell storm and three-dimensional variational method. Mon Weather Rev 141:2759–2777

He Z, Wang D, Qiu X et al (2021) Application of radar data assimilation on convective precipitation forecasts based on water vapor retrieval. Meteorol Atmos Phys 133(3):1–19. https://doi.org/10.1007/s00703-020-00766-x

Hong SY, Dudhia J, Chen SH (2004) A revised approach to ice-microphysical processes for the bulk parameterization of cloud and precipitation. Mon Weather Rev 132:103–120

Hu M, Xue M, Brewster K (2006) 3DVAR and cloud analysis with WSR-88D Level-II data for the prediction of the Fort Worth, Texas, Tornadic thunderstorms. Part I: cloud analysis and its impact. Mon Weather Rev 134:699–721

Kuo YH, Xiao Q, Sun J et al (2005) Assimilation of Doppler radar observations with a regional 3DVAR system: impact of Doppler velocities on forecasts of a heavy rainfall case. J Appl Meteorol Res 44:768–788 2022-02-24

Lee HS (2013) The use of radar data in the metoffice convection-permitting NWP based nowcasting system [EB/OL]. Accessed on 24 feb 2022. http://www2.ucar.edu/for-staff/daily/calendar/2013-09-27/use-radar-data-met-office-convection-permitting-nwp-based

Meng ZY, Zhang FQ (2007) Test of an ensemble Kalman filter for mesoscale and regional-scale data assimilation. Part II: imperfect-model experiments. Mon Weather Rev 135:1403–1423

Meng ZY, Zhang FQ (2008a) Test of an ensemble Kalman filter for mesoscale and regional-scale data assimilation. Part III:

comparison with 3DVAR in a real-data case study. Mon Wea Rev 136:522–540

Meng ZY, Zhang FQ (2008b) Test of an ensemble Kalman filter for mesoscale and regional-scale data assimilation. Part IV: performance over a warm-season month of June 2003. Mon Weather Rev 136:3671–3682

Montmerle T, Faccani C (2009) Mesoscale assimilation of radial velocities from Doppler Radars in a preoperational framework. Mon Weather Rev 137:1939–1953

Noh Y, Cheon WG, Hong SY (2003) Improvement of the K-profile model for the planetary boundary layer based on large eddy simulation data. Bound Layer Meteorol 107:401–427

Schenkman AD, Xue M, Shapiro A et al (2011a) The analysis and prediction of the 8–9 May 2007 Oklahoma tornadic mesoscale convective system by assimilating WSR88D and CASA radar data using 3DVAR. Mon Weather Rev 139(1):224–246

Shen FF, Min JZ (2016) Assimilation of radar radial velocity data with the WRF hybrid ETKF-3DVAR system for the prediction of Hurricane Ike (2008). Atmos Res 169:127–138

Shen FF, Xue M, Xu DM et al (2017a) A comparison between EDAEnVar and ETKF-EnVar data assimilation techniques using radar observations at convective scales through a case study of Hurricane Ike (2008). Meteorol Atmos Phys 130:649–666

Shen FF, Xue M, Min JZ (2017b) A comparison of limited-area 3DVAR and ETKF-En3DVAR data assimilation using radar observations at convective scale for the prediction of Typhoon Saomai 2006. Meteorol Appl 24:628–641

Shen FF, Xu DM, Min JZ (2019a) Effect of momentum control variables on assimilating radar observations for the analysis and forecast for Typhoon Chanthu (2010). Atmos Res 230:104622

Shen FF, Xu DM, Min JZ et al (2019b) Assimilation of radar radial velocity data with the WRF Hybrid 4DEnVar system for the prediction of Hurricane Ike (2008). Atmos Res 234:104771

Sippel JA, Zhang FQ (2008) A probabilistic analysis of the dynamics and predictability of tropical cyclogenesis. J Atmos Sci 65:3440–3459

Skamarock WC, Klemp JB, Dudhia J, Gill DO, Barker DM, Wang, W, Powers JG (2005). A Description of the Advanced Research WRF Version 2 (No. NCAR/TN-468+STR). University Corporation for Atmospheric Research. https://doi.org/10.5065/D6DZ069T

Snyder C, Zhang FQ (2003) Tests of an ensemble Kalman filter for convective-scale data assimilation. Mon Weather Rev 131:1663–1677

Sun J (2005) Initialization and numerical forecasting of a supercell storm observed during STEPS. Mon Wea Rev 133:793–813

Sun J, Wang HL (2013) Radar data assimilation with WRF 4D-Va. Part II: comparison with 3D-Var for a squall line over the U. S. Great Plains. Mon Weather Rev 141:2245–2264

Takemi T (2010) Dependence of the precipitation intensity in mesoscale convective systems to temperature lapse rate[J]. Atmos Res 96(2):273–285

Tanamachi RL, Wicker LJ, Dowell DC et al (2013) EnKF assimilation of high-resolution, mobile Doppler radar data of the 4 May 2007 Greensburg, Kansas, supercell into a numerical cloud model. Mon Weather Rev 141:625–648

Tong M, Xue M (2005) Ensemble Kalman filter assimilation of Doppler radar data with a compressible nonhydrostatic model: OSS experiments. Mon Weather Rev 133:1789–1807

Wang Y, Wang X (2017) Direct assimilation of radar reflectivity without tangent linear and adjoint of the nonlinear observation operator in the GSI-based EnVar system: methodology and experiment with the 8 May 2003 Oklahoma City tornadic supercell. Mon Weather Rev 145:1447–1471

Wang HL, Sun J, Fan S et al (2013a) Indirect assimilation of radar reflectivity with WRF 3D-Var and Its impact on prediction of four summertime convective events. J Appl Meteorol Res Climatol 52:889–902

Wang HL, Sun J, Zhang X et al (2013b) Radar data assimilation with WRF 4D-Var Part I: system development and preliminary testing. Mon Weather Rev 141:2224–2244

Wattrelot E, Caumont O, Mahfouf JF (2014) Operational implementation of the 1D3D-Var assimilation method of radar reflectivity data in the AROME model. Mon Weather Rev 142:1852–1873

Weng YH, Zhang F (2012) Assimilating airborne Doppler radar observations with an ensemble Kalman filter for convection-permitting hurricane initialization and prediction: Katrina (2005). Mon Weather Rev 140:841–859

Weygandt SS, Benjamin SG, Smirnova TG et al. (2008) Assimilation of radar reflectivity data using a diabatic digital filter within the rapid update cycle. Preprint, 12th Conf on IOAS-AOLS, Amer Meteor Soc

Whitaker JS, Hamill TM (2002) Ensemble data assimilation without perturbed observations. Mon Weather Rev 130:1913–1924

Xiao Q, Kuo Y-H, Sun J et al (2005) Assimilation of Doppler radar observations with a regional 3D-Var system: impact of Doppler velocities on forecasts of a heavy rainfall case. J Appl Meteorol 44:768–788

Xiao QN, Kuo YH, Sun JZ (2007a). An Approach of Radar Reflectivity Data Assimilation and Its Assessment with the Inland QPF of Typhoon Rusa (2002) at Landfall. Journal of Applied Meteorology and Climatology 46(1), 14–22.

Xiao QN, Sun JZ (2007b). Multiple-Radar Data Assimilation and Short-Range Quantitative Precipitation Forecasting of a Squall Line Observed during IHOP_2002. Mon Weather Rev 135(10), 3381–3404.

Xue M, Droegemeier KK, Wong V (2000) The advanced regional prediction system (ARPS)—a multi-scale nonhydrostatic atmospheric simulation and prediction tool. Part I: model dynamics and verification. Meteorol Atmos Phys 75:161–193

Xue M, Wang DH, Gao JD et al (2003) The advanced regional prediction system (ARPS), storm-scale numerical weather and data assimilation. Meteorol Atmos Phys 82:139–190

Xue M, Tong M, Droegemeier KK (2006) An OSSE framework based on the ensemble square-root Kalman filter for evaluating impact of data from radar networks on thunderstorm analysis and forecast. J Atmos Oceanic Technol 23:46–66

Zhang J (1999) Moisture and diabatic initialization based on radar and satellite observations dissertation. University of Oklahoma, Oklahoma

Zhang FQ, Sippel JA (2009) Effects of moist convection on hurricane predictability. J Atmos Sci 66:1944–1961

Zhang FQ, Weng YH (2014) Modernizing the prediction of hurricane intensity and associated hazards: a five-year real-time forecast experiment concluded by superstorm Sandy (2012). Bull Amer Meteorol Soc 96:25–33

Zhang FQ, Snyder C, Rotunno R (2004) Tests of an ensemble Kalman filter for convective-scale data assimilation: Impact of initial estimate and observations. Mon Weather Rev 132:1238–1253

Zhang FQ, Odins AM, Nielsen-Gammon JW (2006a) Mesoscale predictability of an extreme warm-season precipitation event. Weather Forecast 21:149–166

Zhang FQ, Meng ZY, Aksoy A (2006b) Test of an ensemble Kalman filter for mesoscale and regional-scale data assimilation. Part I: perfect-model experiments. Mon Weather Rev 134:722–736

Zhang FQ, Weng YH, Sippel AJ et al (2009) Convection-permitting hurricane initialization and prediction through assimilation of Doppler radar observations with an ensemble Kalman filter: Humberto (2007). Mon Wea Rev 137:2105–2125

Zhao K, Xue M (2009) Assimilation of coastal Doppler radar data with the ARPS 3DVAR and cloud analysis for the prediction of Hurricane Ike (2008). Geophys Res Lett 36:L12803. https://doi.org/10.1029/2009GL038658